K-J POLAR ANGULAR QUADRATURE SET FOR A METHOD OF CHARACTERISTICS BASED ON NEUTRON SCATTERING CROSS-SECTIONS

by

Donghoon KIM, Lucas I. ALBRIGHT, Brittney L. SAENZ, and Tatjana JEVREMOVIC *

University of Utah Nuclear Engineering Program, Salt Lake City, Utah, USA

Scientific paper
https://doi.org/10.2298/NTRP181021002K

A novel polar angular quadrature set called the Kim-Jevremovic polar angular quadrature set is derived for the method of characteristics. It is based on neutron anisotropic scattering cross-sections in the Evaluated Nuclear Data File. This new set is implemented within the state-of-the-art neutron transport code AGENT and tested in comparison to MCNP6 as well as to other known quadrature sets for the UO_2 unit cells, the well-known C5G7 benchmark, unreflected cylinders of uranyl-fluoride solutions in heavy water, and the University of Utah 100 kW_{th} TRIGA MARK-I reactor core. These comparisons show that the newly proposed polar angular quadrature set provides better agreements than other quadrature sets for the lower order of anisotropic scattering expansions. This paper presents a complete derivation of the Kim-Jevremovic polar angular quadrature set and the analysis for the mentioned benchmark examples.

Key words: AGENT code, method of characteristics, neutron anisotropic scattering, polar angular quadrature set, C5G7 benchmark, TRIGA

INTRODUCTION

The method of characteristics (MOC) is considered to be currently one of the most accurate 3-D deterministic solutions to the neutron transport equation [1]. With the MOC, the heterogeneous geometries can be described without approximations relying on a robust ray tracing mimicking neutron motion along the 3-D trajectories. The MOC therefore requires weighted azimuthal and polar angles to describe neutron motion in 3-D. The azimuthal angles are usually uniformly distributed in space while the polar angular quadrature set consists of the selected polar angles and their associated weights for optimizing the calculation time. The common quadrature sets are Gauss-Legendre (GL) [2], CACTUS [3], Leonard and McDaniel (LM) [4], and the recently developed Tabuchi-Yamamoto (TY) [5] demonstrating a certain level of accuracy for various types of reactor core complexities [4, 6, 7]. One method of modeling the neutron anisotropic scattering as explicitly as doable within the MOC is based on the expansion of the scattering source term using the Legendre polynomials. The greater accuracy achieved with the Legendre polynomials requires greater computational times because the higher (and more accurate) orders of the Legendre polynomial expansion must be added in the scattering source term to account for the anisotropy of neutron scattering. Some of the most used MOC codes that include anisotropic scattering approximation based on Legendre polynomials are DRAGON [8], NELAT [9] and AGENT [10, 11]. These codes include one or more of the polar angle quadrature sets as GL, CACTUS, and LM.

The Kim-Jevremovic (*K-J*) polar angle quadrature set is developed to account for neutron anisotropic scattering and provides required accuracy for the lower orders of the Legendre polynomial expansion, thus reducing computational time. It is used within the AGENT code in synergism with other polar angle quadrature sets. Namely, the *K-J* set is developed for coolant regions containing hydrogen or deuterium using the ENDF-VII library data [12] for differential elastic scattering of a neutron of various energies; while, in the fuel region currently any other polar angular quadrature set can be used. The *K-J* polar angular quadrature set derived for light and heavy water uses the same polar angles as the LM scheme. The same derivation is also provided for the *K-J* polar angular quadrature set with the TY scheme for the light water moderator.

* Corresponding author; e-mail: T.Jevremovic@iaea.org

DERIVATION OF THE *K-J* POLAR ANGLE QUADRATURE SET

The *K-J* polar angle quadrature set for the light water coolant

The *K-J* polar angular quadrature set is a weighting scheme that can be applied to other polar angular quadrature sets. The *K-J* weighting function is derived from differential cross-sections for elastic scattering of neutrons with hydrogen (^{1}H) for various incident neutron energies; derivation is based on the ENDF-VII library with the Legendre function of the first kind [13]. The ^{1}H is the most dominant nucleus in the coolant of Light Water Reactors (LWR). Moreover, neutron elastic scattering interactions are the most dominant interactions with ^{1}H, as shown in fig. 1.

Figure 2 shows differential cross-sections for elastic neutron scattering, $d\sigma_i/d\Omega_i$, with ^{1}H for various neutron energies created using the Legendre expansion coefficient provided in the ENDF-VII library. The Legendre polynomial coefficients can approximate a function with the orthogonality between [–1, +1]. The series can be expressed as follows [14]

$$f(\mu,E,E') \quad \sum_{l\ 0}^{NA} \frac{2l\ \ 1}{2}\alpha_l(E,E')P_l(\mu) \qquad (1)$$

where $f(\mu\ E\ E'$ probability distribution as a function of incident neutron energy E, energy E' of the emitted neutron, and the cosine of the angle in which the neutron is emitted μ, NA is the maximum order of the Legendre polynomial expansion, α_l the Legendre expansion coefficient that is tabulated as a function of incident neutron energy, and l – the Legendre expansion coefficients.

Legendre functions of the first kind, also called the Legendre polynomial, P_n order, or zonal harmonics, are a solution to the Legendre differential eq. (2)

$$(1\ \ x^2)\frac{d^2y}{dx^2}\ \ 2x\frac{dy}{dx}\ \ \ n(n\ \ 1)\ \ \frac{m^2}{1\ \ x^2}\ \ y\ \ \ 0 \qquad (2)$$

The first few Legendre functions of the first kind are

$$P_0(x)\ \ \ 1, P_1(x)\ \ \ x, P_2(x)\ \ \frac{1}{2}(3x^2\ \ \ 1), P_3(x)$$
$$\frac{1}{2}(5x^3\ \ \ 3x)P_4(x)\ \ \frac{1}{8}(35x^4\ \ \ 30x^2\ \ \ 3), P_5(x)$$
$$\frac{1}{8}(63x^5\ \ \ 70x^3\ \ \ 15x)\ldots \qquad (3)$$

Figure 3 shows the first few Legendre functions of the first kind from P_0 to P_5. The differential cross-sections for elastic neutron scattering (*e. g.* fig. 2) can be derived from the ENDF-VII library based on the Legendre function of the first kind [13]. In the *K-J* polar angular quadrature set, the weighting factor for a given polar angle is defined as the ratio between the chosen differential cross-section and the sum of all differential cross-sections of a given energy, calculated as follows

$$w(i)\ \ \frac{d\sigma_i/d\Omega_i}{\sum_{i=1}^{N} d\sigma_i/d\Omega_i}, i\ \ \ 1\ldots N \qquad (4)$$

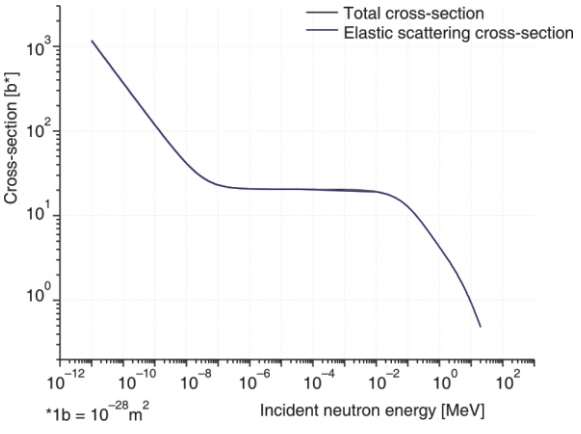

Figure 1. Total and elastic neutron scattering cross-sections for hydrogen (1H) [12]

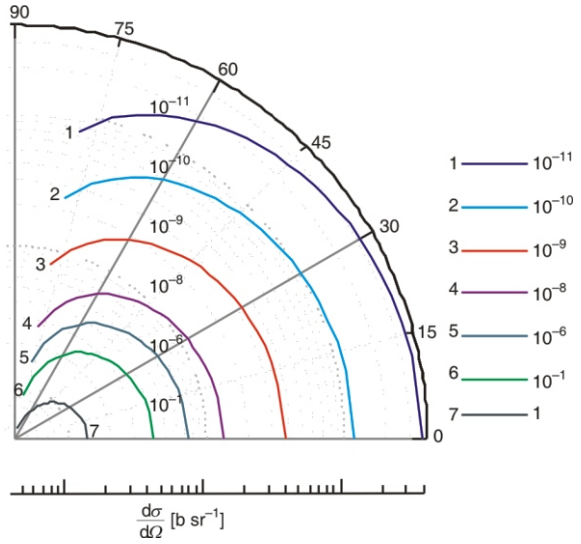

Figure 2. Differential cross-section for neutron elastic scattering on ^{1}H in units of barn per steradian for various neutron energies [12]

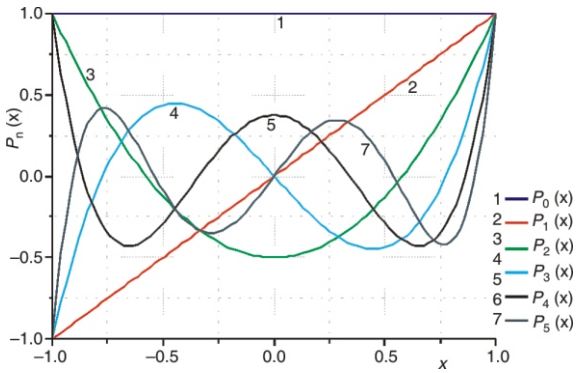

Figure 3. Legendre functions of the first kind

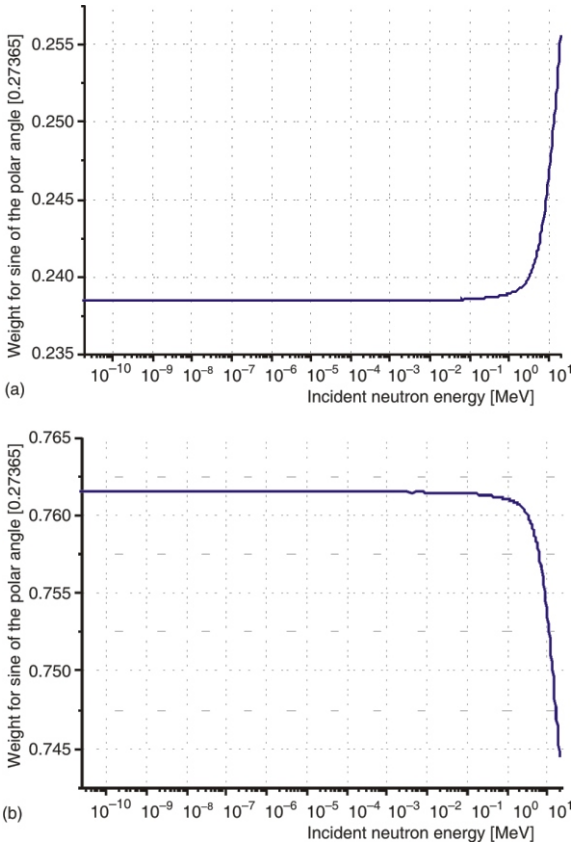

Figure 4. The *K-J* polar angle quadrature weighting value per neutron energy of ^{1}H for two polar angles with (a) sin(θ) = 0.27365, (b) sin(θ) = 0.86571

The *K-J* quadrature set can also be described as a fitting function of the weight of the polar angles and incident neutron energy, as shown for $N = 2$ polar angles (this is also shown in fig. 4)

$$w(E)$$
$$0.23852 \quad 0.00045133\ E^{1.07282}, \sin\theta \quad 0.273658$$
$$0.76148 \quad 0.00045133\ E^{1.22642}, \sin\theta \quad 0.865714 \tag{5}$$

where w is the weight of the polar angle and E – the incident neutron energy [MeV]

In the *K-J* polar angular quadrature set, selected angles are weighted by the relative differential elastic scattering cross-section for ^{1}H, as shown in fig. 2. The *K-J* polar angular quadrature set should only be utilized in the regions where elastic scattering with ^{1}H is the most dominant interaction, such as the light water moderator. Therefore, the *K-J* polar angular quadrature set for differential elastic scattering with hydrogen cannot be applied to other moderators such as graphite or heavy water.

The *K-J* polar angle quadrature set for the heavy water coolant

Much like the *K-J* polar angular quadrature set derived for ^{1}H, the *K-J* weighting function for deuterium (^{2}H) is derived using the differential cross-sections for the elastic scattering of neutrons with ^{2}H at various incident neutron energies. This derivation is also based on the ENDF-VII library with the Legendre function of the first kind [13]. Neutron elastic scattering interactions with ^{2}H are the dominant one as shown in fig. 5.

The differential cross-sections for elastic neutron scattering ($d\sigma_i/d\Omega_i$) with ^{2}H calculated using the Legendre expansion coefficient for various neutron energies, as provided by the ENDF-VII library, is shown in fig. 6. The differential cross-section for neutron elastic scattering on a ^{2}H is more isotropic at low incident neutron energies than for ^{1}H. Elastic scattering on ^{1}H always demonstrates forward-bias anisotropic scattering due to the equivalent mass between a ^{1}H and a neutron, making it less isotropic than the scattering on a ^{2}H. The differential cross-section for neutron elastic scattering at high incident neutron energies, however, shows anisotropic scattering for both ^{1}H and ^{2}H.

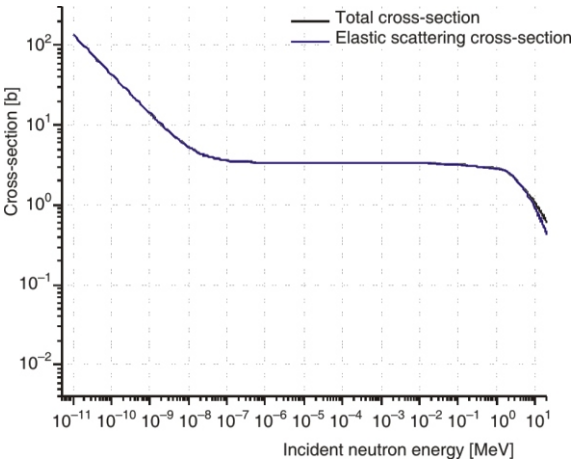

Figure 5. Total and elastic neutron scattering cross-sections for ^{2}H based on the ENDDB-VII library [12]

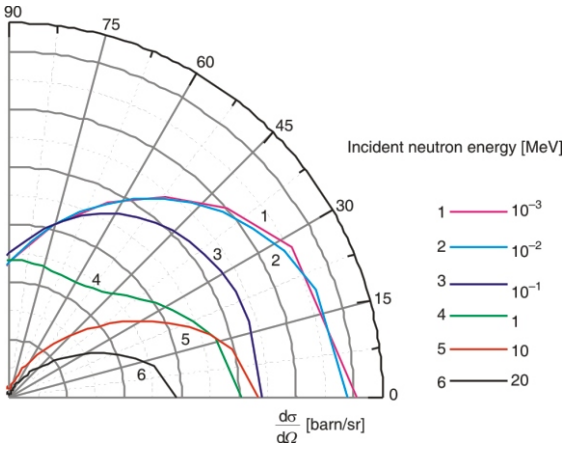

Figure 6. Differential cross-section for neutron elastic scattering on ^{2}H in units of barn per steradian for various neutron energies [12]

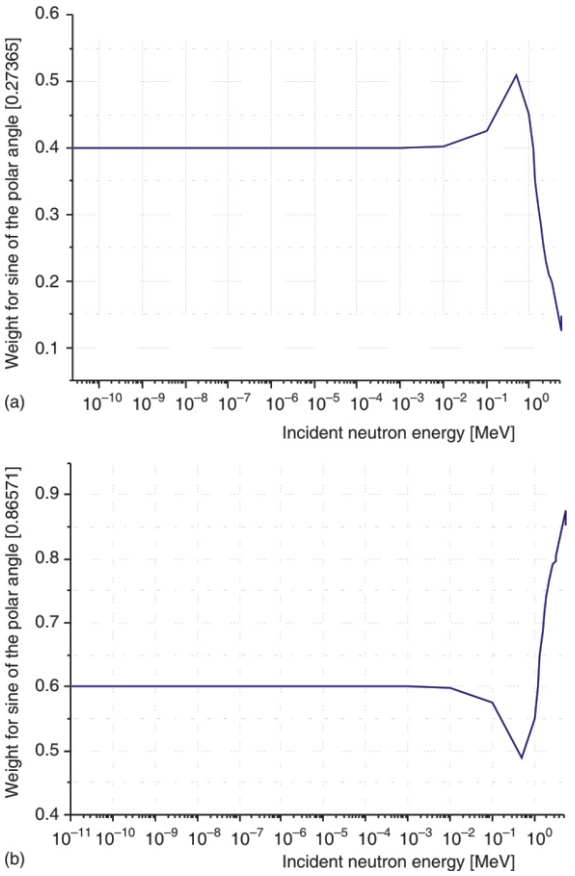

Figure 7. The *K-J* polar angle quadrature weighting value per neutron energy of ^{2}H for two polar angles with (a) sin(θ) = 0.86571 and (b) sin(θ) = 0.27365

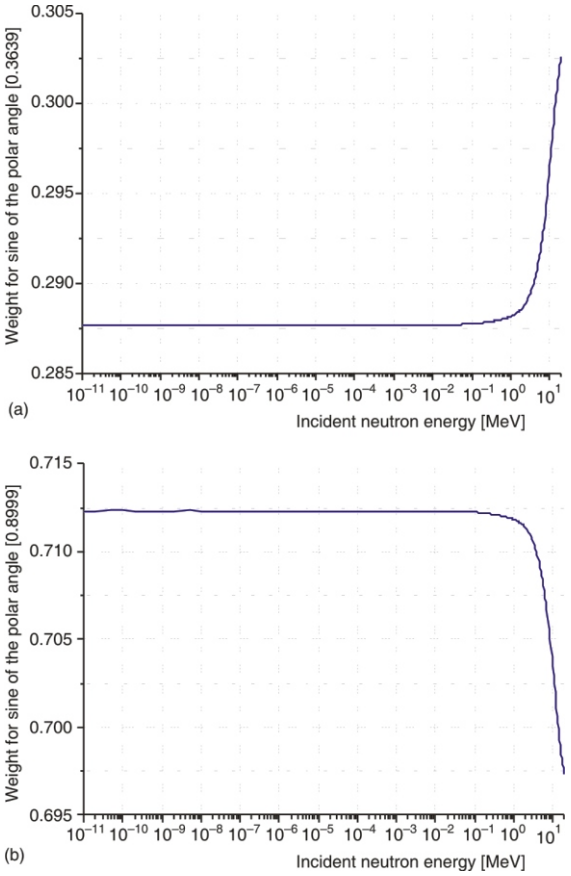

Figure 8. The *K-J* polar angle quadrature weighting value per neutron energy of ^{1}H for TY polar angles with (a) sin(θ) = 0.8999 and (b) sin(θ) = 0.3639

Angles used in the *K-J* polar angular quadrature set are weighted by the relative differential elastic scattering cross-sections for ^{2}H, as shown in fig. 7. Compared to the *K-J* polar angle quadrature weighting value per neutron energy of ^{1}H (0.75~0.76), the *K-J* polar angle quadrature set of ^{2}H shows greater fluctuation (0.48~0.85) with incident neutron energy. This difference is observed because the differential cross-section for neutron elastic scattering on ^{1}H always shows forward-bias anisotropic scattering, due to the equivalent mass between a ^{1}H and a neutron, even at low incident energies.

The *K-J* polar angle quadrature set for the light water coolant with ty polar angles

The *K-J* polar angular quadrature set for the light water coolant with TY polar angles are based on the differential cross-sections for elastic neutron scattering (*e. g.* fig. 2) derived from the ENDF-VII library based on the Legendre function of the first kind [13]. In the *K-J* polar angular quadrature set, the weighting factor for a given polar angle from the TY polar angle quadrature set is defined as the ratio between the chosen differential cross-section and the sum of all differential cross-sections of a given energy, eq. (4). The *K-J* quadrature set can also be described for $N = 2$ from the TY polar angles in fig. 8.

Comparisons of the polar angles quadrature sets angles and their respective weights

Table 1 shows polar angles and their associated weights for six different polar angle quadrature sets: GL, CACTUS, LM, TY, *K-J* for ^{1}H with LM angles, *K-J* for ^{1}H with TY angles, and *K-J* for ^{2}H with LM angles. Theoretically, it is possible to use any set of polar angles and weights, given that the sum of their weights equals one. Figure 9 shows how *K-J* for ^{1}H, ^{2}H with LM angles and *K-J* for ^{1}H with TY angles compares to LM, TY, GL, and CA polar angular quadrature sets for two polar angles-values and their associated weights. Additionally, unlike the GL and CACTUS polar angle quadrature sets, the *K-J* polar angular quadrature set gives greater weight to larger polar angles than to smaller polar angles. This is achieved by weighting polar angles by their relative differential cross-sections for elastic scattering (illustrated in fig. 9). Compared to the LM polar angular quadrature set, the *K-J* polar angular quadrature set with both ^{1}H and ^{2}H uses the same polar angles while applying less weight to larger polar angles and greater weight to smaller polar angles.

Table 1. Comparison of GL, CACTUS, LM, TY, *K-J* polar angular quadrature sets

Method	Parameter	Number of polar angles		
		1	2	3
Gauss-Legendre	Sinθ [(a)]	0.577350	0.339981, 0.861136	0.238619, 0.661209, 0.932469
	w	1.0	0.652145, 0.347854	0.467913, 0.360761, 0.171324
CACTUS	Sinθ	0.618990	0.416984, 0.873287	0.291366, 0.698869, 0.941120
	w	1.0	0.707106, 0.292893	0.500000, 0.366025, 0.133974
Leonard and McDaniel	Sinθ	0.752244	0.273658, 0.865714	0.103840, 0.430723, 0.905435
	w	1.0	0.139473, 0.860527	0.020530, 0.219161, 0.760309
Tabuchi and Yamamoto	Sinθ	0.798184	0.363900, 0.899900	0.166648, 0.537707, 0.932954
	w	1.0	0.212854, 0.787146	0.046233, 0.283619, 0.670148
Kim and Jevremovic for ^{1}H with Leonard and McDaniel angles	Sinθ	0.752244	0.273658, 0.865714	0.103840, 0.430723, 0.905435
	w [(b)]	1.0	0.241178, 0.758813	0.136076, 0.280513, 0.583393
Kim and Jevremovic for ^{1}H with Tabuchi and Yamamoto angles	Sinθ	0.798184	0.363900, 0.899900	0.166648, 0.537707, 0.932954
	w [(b)]	1.0	0.290278, 0.709722	0.124334, 0.322057, 0.553609
Kim and Jevremovic for ^{2}H with Leonard and McDaniel angles	Sinθ	0.752244	0.273658, 0.865714	0.103840, 0.430723, 0.905435
	w [(b)]	1.0	0.264997, 0.735002	0.168732, 0.226883, 0.604384

[(a)] angle (θ) is the polar angle measured from the z-axis, [(b)] energy-averaged weighting factor (w) for the *K-J* polar angular quadrature set

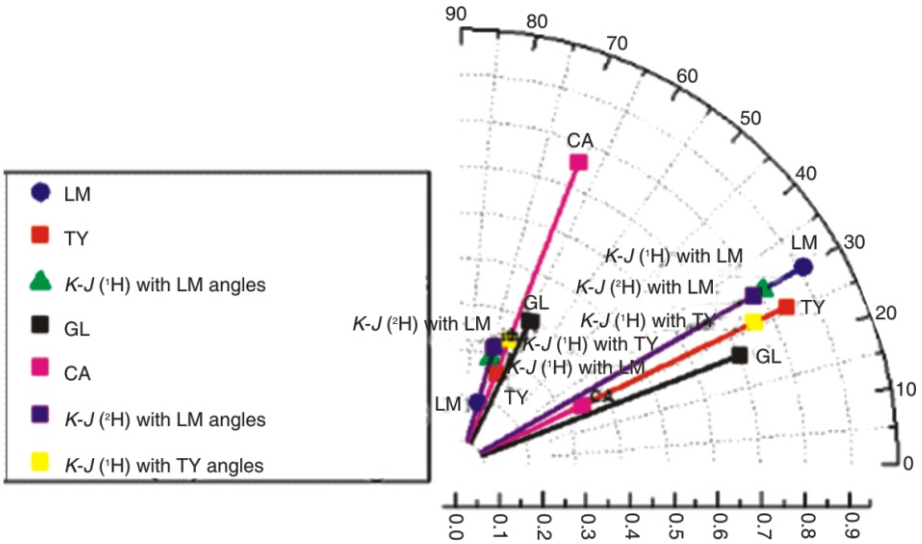

Figure 9. Comparison of *K-J*, LM, TY, GL, and CA polar angles and their associated weights

VERIFICATION OF THE *K-J* POLAR ANGULAR QUADRATURE SET

The *K-J* polar angular quadrature set is compared to two other polar angular quadrature sets available in AGENT (LM and TY) for the four different benchmark examples: square unit cell, 2-D C5G7 benchmark, unreflected cylinders of uranyl-fluoride solutions in heavy water, and 3-D University of Utah TRIGA MARK-I reactor (3-D UUTR benchmark). The AGENT based analysis for each benchmark example is based on the TY and LM polar angular quadrature set for all material regions except the *K-J* polar angular quadrature which is used in the moderator region.

The 2-D square unit cell

The 2-D square unit cell is based on the Venus-2 unit cell benchmark [15]; data are provided in tab. 2 and the unit cell geometry is shown in fig. 10. The AGENT model includes LM, TY, and *K-J* polar angular quadrature sets with two polar angles and 44 energy group cross-sections derived from SCALE 6.2.1. The number of azimuthal angles, ray separation, sub-mesh option, and the number of boundary edges are shown in tab. 3, from where also it can be seen that the *K-J* polar angular quadrature set has the best agreement with the MCNP6. With the P_n order increased, the percent difference compared to MCNP6 reduces. Computation times among the four polar angular quadrature sets (*K-J*, LM, and TY) are comparable, with no polar angular quadrature set demonstrating superior computational efficiency. The difference between the MCNP6 reference and AGENT calculation for P2 with the *K-J* polar angular quadrature set (0.06 %) provides comparable agreement than P_4 with the LM (0.04 %) and TY (0.05 %) polar angular quadrature set. All differences between the MCNP6 reference and AGENT calculations are below 1 %.

Table 2. Material compositions of the unit cell shown in fig. 10

Unit cell region	Element	Number density [cm^{-3}]
Fuel	^{234}U	6.74213 10^{18}
	^{235}U	7.65322 10^{20}
	^{236}U	3.68820 10^{18}
	^{238}U	2.20912 10^{22}
	O	4.57338 10^{22}
	^{10}B	3.64042 10^{17}
	^{11}B	1.46531 10^{16}
Cladding	Cr	7.69688 10^{19}
	Fe	1.43323 10^{20}
	Sn	4.75354 10^{20}
	O	3.00167 10^{20}
	Zr	4.30680 10^{22}
Moderator	H	6.68559 10^{22}
	O	3.34279 10^{22}

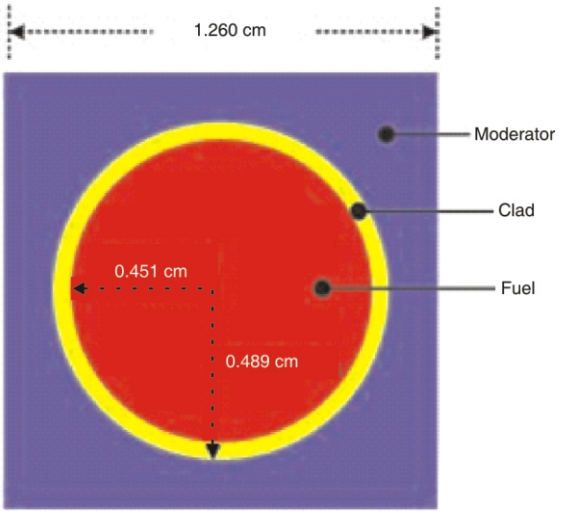

Figure 10. Unit cell geometry [15]

Table 3. AGENT k_{inf} values for the 3.3 wt. % enriched UO_2

Method		P_0	P_1	P_2	P_3	P_4	P_5
AGENT with LM	k_{inf}	1.378728	1.378727	1.385419	1.385418	1.386361	1.386495
	CPU time [s]	49	67	72	78	84	101
	Difference [%]	0.60	0.61	0.12	0.12	0.05	0.05
AGENT with TY	k_{inf}	1.378505	1.378504	1.385251	1.385209	1.386152	1.386287
	CPU time [s]	50	69	73	80	85	100
	Difference [%]	0.62	0.62	0.13	0.14	0.07	0.06
AGENT for *K-J* with LM angles in moderator region and LM in fuel/cladding region	k_{inf}	1.379407	1.379406	1.386005	1.386004	1.386942	1.387075
	CPU time [s]	54	72	75	82	88	100
	Difference [%]	0.56	0.56	0.08	0.08	0.01	0.00
AGENT for *K-J* with TY angles in moderator region and TY in fuel/cladding region	k_{inf}	1.378862	1.378862	1.385517	1.385517	1.386458	1.386592
	CPU time [s]	57	68	76	80	88	105
	Difference [%]	0.60	0.60	0.12	0.12	0.05	0.04
MCNP6	k_{inf} (reference)	1.38712 0.00002					
	CPU time [s]	3280					

AGENT resolution parameters: 48 azimuthal angles, 2 polar angles, 0.004 cm ray separation, 12 boundary edges per side
AGENT converging criteria: for flux 10^{-6}, for eigenvalue 10^{-6}
Boundary condition: reflective boundary condition
MCNP6 parameters: 100,000 particles, 110 histories, ENF/B-VII.0
Difference (%) = absolute (100 × (kinf (MCNP6) – k_{inf} (AGENT)) / (kinf (MCNP6)))
Computer: Intel Xeon x5660 processor, 2.8 Ghz speed

AGENT sub-meshing of the unit cell:

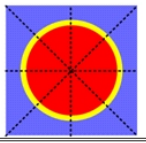

Figures 11 and 12 compare the P_0 angular neutron flux distributions between the *K-J* and LM polar angular quadrature sets in selected locations within the moderator and fuel regions for different neutron energy groups. There are four selected locations in the moderator region and five selected locations in the fuel region. The fast neutron energy group is represented by the energy range 1.85 MeV < E < 2.354 MeV, and the thermal neutron energy group is represented by the energy range 10^{-2} eV < E < 2.53 10^{-2} eV.

Figure 11 shows a comparison of the P_0 angular neutron flux distributions between the *K-J* and LM polar angular quadrature sets for the thermal energy group. The thermal angular neutron flux distribution with the *K-J* polar angular quadrature set in both the moderator and fuel regions match closely. The thermal angular neutron flux with the *K-J* polar angular quadrature set is larger compared to the LM polar angular quadrature set. Figure 12 shows a comparison of the P_0 angular neutron flux distributions between the *K-J* and LM polar angular quadrature sets for the fast energy group. The fast angular neutron flux distribution of the *K-J* polar angular quadrature set in both the moderator and fuel regions also match closely. Differences in the magnitudes of the normalized fast angular neutron flux between the *K-J* and LM polar angular quadrature sets are approximately 10^{-6}, with the *K-J* polar angular quadrature set again being smaller. The largest differences between the *K-J* and LM polar angular quadrature sets are observed in the four locations within the moderator region, as expected. Furthermore, because the *K-J* and LM polar angular quadra-

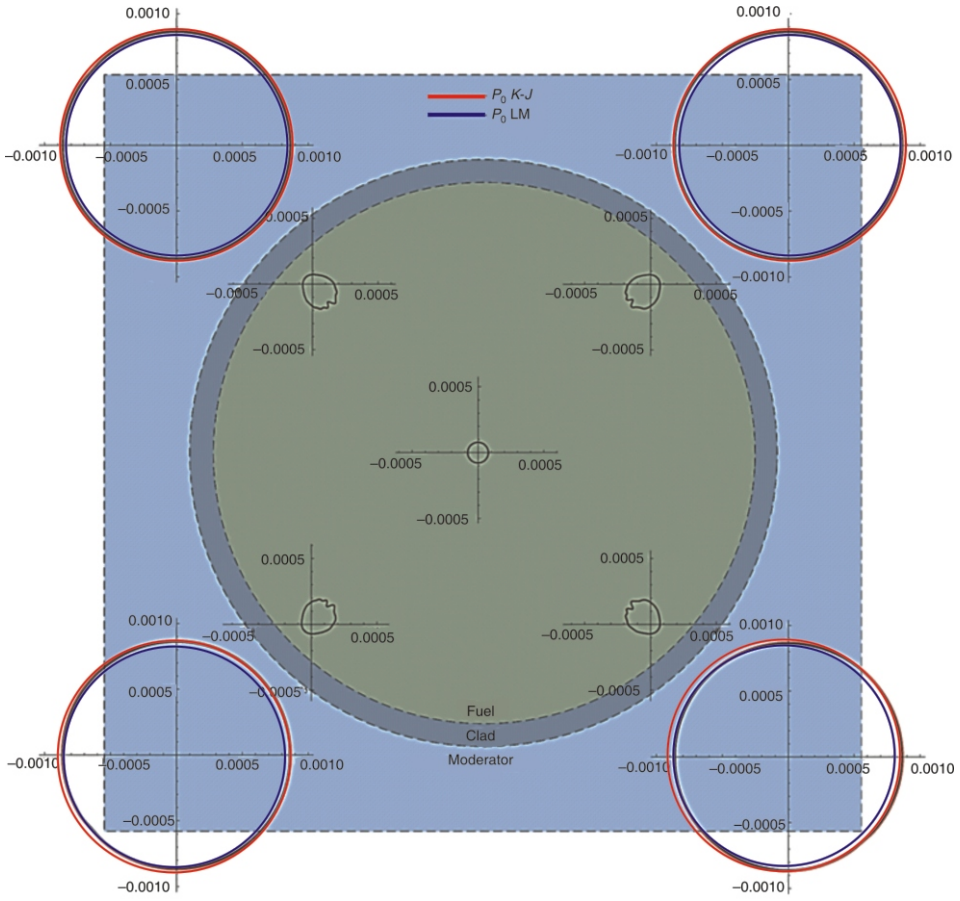

Figure 11. The P_0 angular neutron flux distributions of the *K-J* and LM polar angular quadrature sets in the 3.3 wt. % enriched UO_2 unit cell for thermal energy group (10^{-2} eV < *E* < 2.53 10^{-2} eV)

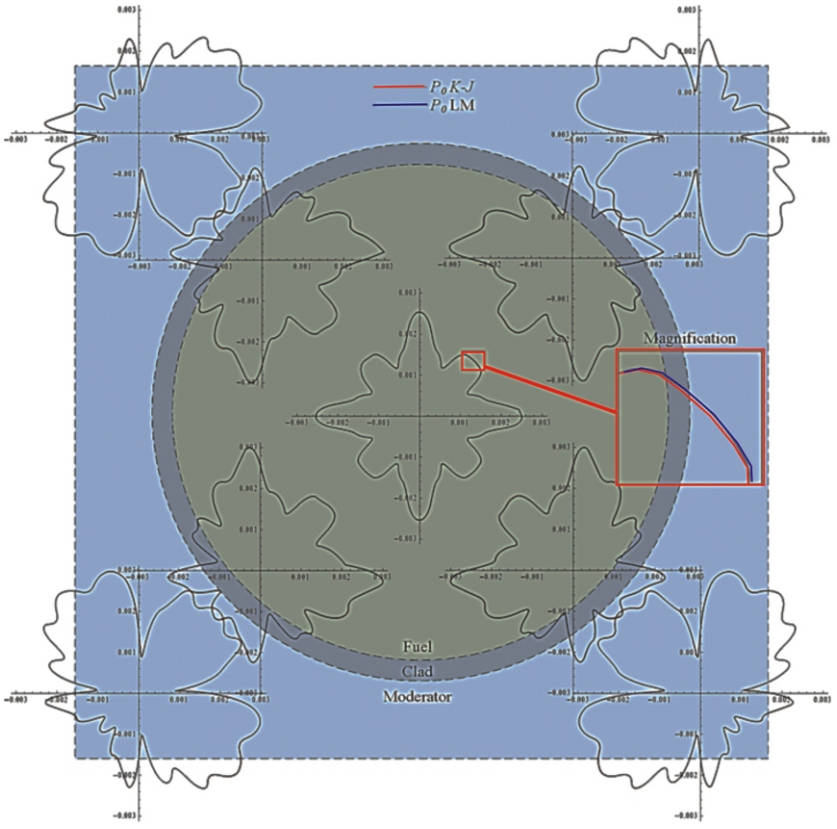

Figure 12. The P_0 angular neutron flux distributions of the *K-J* and LM polar angular quadrature sets in the 3.3 wt. % enriched UO_2 unit cell for fast energy group (1.85 MeV < *E* < 2.354 MeV)

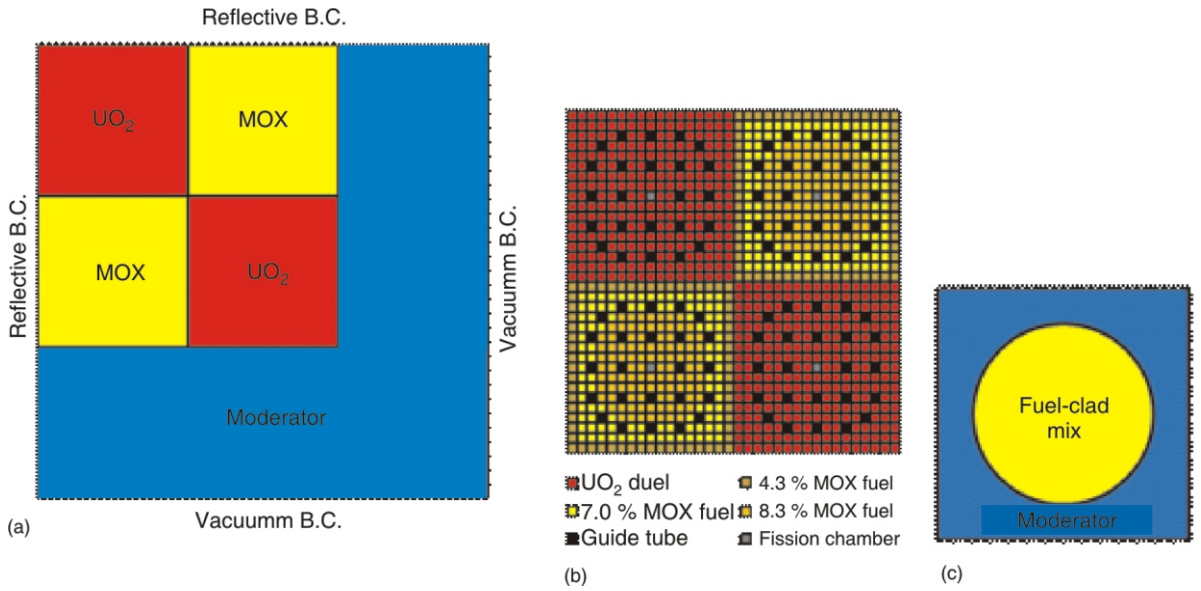

Figure 13. The 2-D C5G7 Benchmark geometry (a) core description (b) fuel assemblies (c) fuel pin [16]

Table 4. The AGENT k_{eff} values for the 2-D C5G7 benchmark

Method		P_0	P_1	P_2	P_3	P_4	P_5
AGENT with LM	k_{eff}	1.21784	1.21777	1.21814	1.21814	1.21820	1.21822
	Difference [%]	3.41	3.40	3.43	3.43	3.44	3.44
	CPU time (hrs)	6	6.5	7.5	9	10	11
AGENT with TY	k_{eff}	1.17504	1.17489	1.17527	1.17528	1.17533	1.17535
	Difference [%]	0.23	0.24	0.21	0.21	0.20	0.20
	CPU time (hrs)	6	6.5	7.5	9	10	11
AGENT with *K-J* in moderator region and LM in fuel/cladding region	k_{eff}	1.17673	1.17659	1.17696	1.17696	1.17702	1.17704
	Difference [%]	0.08	0.09	0.06	0.06	0.06	0.06
	CPU time (hrs)	6	6.5	7.5	9	10	11
MCNP6	k_{inf} (reference)	1.17771 0.00003					
	CPU time [s]	18.5					
AGENT resolution parameters: 48 azimuthal angles, 2 polar angles, 0.01 cm ray separation, 204 boundary edges per side AGENT converging criteria: for flux 10^{-6}, for eigenvalue 10^{-6} Boundary condition: reflective & vacuum boundary condition MCNP6 parameters: 1.000.000 particles, 600 histories, ENF/B-VII.0 Difference (%) = absolute (100 × (k_{inf} (MCNP6) – k_{inf} (AGENT)) / (k_{inf} (MCNP6))) Computer: Intel Xeon 5660 processor, 2.8 Ghz speed		AGENT sub-meshing of the unit cells: 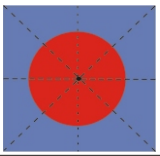					

ture sets use the same polar angles, the observed differences in the moderator region are due to the different weightings for these polar angles.

The 2-D C5G7

The 2-D C5G7 benchmark example [16] is a 2 2 MOX and UO_2 fuel assembly core surrounded with the reflector region. The overall dimensions, as shown in fig. 13(a), are 64.26 cm 64.26 cm. The vacuum boundary conditions are applied to the right side and the bottom of the core while the reflective boundary conditions are applied to the top and left side of the core. Figure 13(b) shows dimensions of four fuel assemblies that are each 21.42 cm 21.42 cm and consist of 17 17 lattices of square pin cells. The unit cell pitch is 1.26 cm and consists of a cylinder of radius 0.54 cm representing homogenized fuel-clad mixtures or guide tubes and water moderator, as shown in fig. 13(c); the same water composition is used for the moderator surrounding the fuel assemblies.

The AGENT calculations model of the 2-D C5G7 benchmark compares LM, TY, and *K-J* polar angular quadrature sets with two polar angles and seven energy group cross-sections [16]. The *K-J* polar angular quadrature sets with LM angles is are selected. Table 4 summarizes the AGENT kinf values for $P_0 \sim P_5$ for all three polar angular quadrature sets, as well as the MCNP6 reference values. It can be seen that the *K-J* polar angular quadrature set provides the best agreement compared to MCNP6 for all P_n orders ($P_0 \sim P_5$). Also, the *K-J* polar angular quadrature set with higher P_n order shows best agreement with the MCNP6. All differences between the MCNP6 and AGENT are below 3.4 %, and differences between the

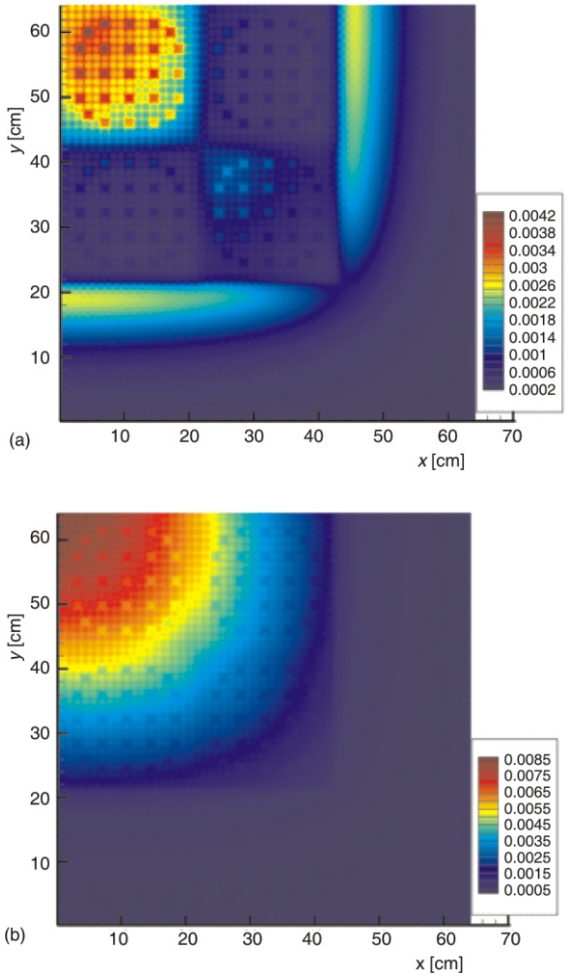

Figure 14. The AGENT normalized P_5 scalar flux distribution for the 2-D C5G7 benchmark: (a) thermal neutron energy group (10^{-5} ~ 0.125 eV) (b) fast neutron energy group (1.356 10^6 ~ 2 10^7 eV)

MCNP6 and the *K-J* polar angular quadrature set are 0.09 %. All three polar angular quadrature sets show similar computation time for all P_n orders ($P_0 \sim P_5$). The difference between the MCNP6 reference and AGENT for P_1 with the *K-J* polar angular quadrature set (0.09 %) provides better agreement than P_5 with the LM (3.4 %) and TY (0.2 %) polar angular quadrature set. These results demonstrate that the accuracy of the MOC methods can be improved with the *K-J* quadrature set and with shortening the computational time to half.

Figures 14(a) and 14(b) show P_5 scalar neutron flux for the *K-J* polar angular quadrature set for thermal ($10^{-5} \sim 0.125$ eV) and fast ($1.356\ 10^6 \sim 2\ 10^7$ eV) energy groups, respectively. Within the fuel assemblies, the thermal scalar neutron flux fig. 14(a) is highest in the guide tube and the moderator-filled interstitial spacing between fuel rods due to elastic scattering interactions with the ^{1}H. The thermal scalar neutron flux is lowest in the fuel rods due to neutron absorptions, such as fission and radiative capture, in the fuel. The thermal scalar neutron flux is larger in both UO_2 fuel assemblies than in the MOX fuel assemblies, with the highest thermal scalar neutron flux values in the upper-left UO_2 fuel assembly. In the moderator external to the C5G7 core, a greater thermal scalar neutron flux with a local maximum occurs immediately beyond the core boundary. The increased thermal scalar neutron flux observed at the boundary of the core tapers from maximum values along the reflective boundaries (top and left-hand side of the geometry) to smaller values at the bottom right corner of the C5G7 core. Beyond the local maximum, the thermal scalar neutron flux decreases in the directions of the vacuum boundaries (bottom and right-hand side of the problem geometry). As expected, the thermal scalar neutron flux generally decreases with distance from the upper-left corner of the C5G7 core where the fuel assemblies are located, and the top and left-hand side reflective boundary conditions meet.

The fast neutron scalar flux fig. 14(b) is greatest within the fuel assemblies, with the highest values in the fuel rods, where fast neutrons are born from fission. Within the fuel assemblies, the magnitude of the fast scalar neutron flux is smaller in the empty guide tube positions and the moderator-filled interstitial spacing between fuel rods, where elastic scattering interactions with the moderator thermalize neutrons. Furthermore, the fast neutron scalar flux within the fuel assemblies decreases with distance from the reflective boundary conditions (top and left-hand side of the problem geometry) towards the vacuum boundary conditions (bottom and right-hand side of the problem geometry). A steep gradient in the fast neutron scalar flux is observed at the boundary between the C5G7 core and the moderator region external to the C5G7 core. Within the moderator region external to the C5G7 core, the fast neutron scalar flux remains at a minimum because no fast neutrons are produced in the moderator.

Unreflected cylinders of uranyl-fluoride solutions in heavy water

The unreflected cylinders of uranyl-fluoride solutions in heavy water [17] are selected to verify the *K-J* polar angular quadrature set for the regions with ^{2}H. This benchmark example was developed by the Los Alamos Scientific Laboratory to investigate critical parameters of enriched uranyl-fluoride (UO_2F_2) heavy-water solutions for a fixed ^{2}H-to-^{235}U atomic ratio. The benchmark consists of heavy water reflected cylinders of uranyl fluoride in which the atomic ratio of ^{2}H to ^{235}U is 210. Outside of the wall, the model assumes vacuum boundary conditions. The overall dimensions of the unreflected cylinders of uranyl-fluoride solutions in heavy water are shown in fig. 15. The material compositions are shown in tab. 5.

The AGENT model of the unreflected cylinders of uranyl-fluoride solutions in heavy water is devel-

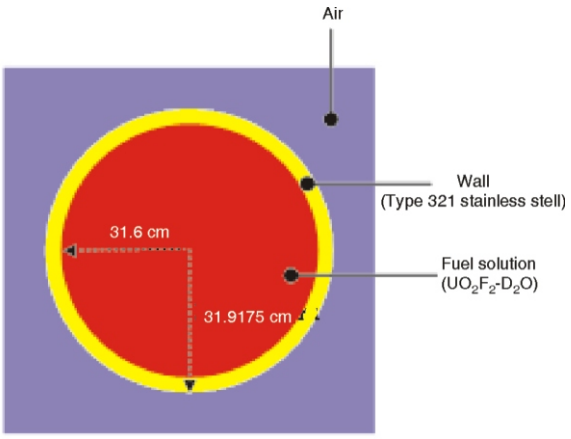

Figure 15. Unreflected cylinders of uranyl-fluoride solutions in heavy water

oped to compare the LM, TY, and *K-J* polar angular quadrature sets using two polar angles and seven energy group cross-sections [16]. Table 6 summarizes the AGENT k_{eff} values for $P_0 \sim P_5$ for all three polar angular quadrature sets, compared to the MCNP6 reference. The *K-J* polar angular quadrature set provides the best agreement with MCNP6 for all P_n orders ($P_0 \sim P_5$); the best agreement with the reference is also found for higher P_n orders. The differences observed between the MCNP6 reference and AGENT calculations are <8.67 %, and differences between the MCNP6 and the *K-J* polar angular quadrature set are 0.35 %. All three polar angular quadrature sets have the same computation time for all P_n orders ($P_0 \sim P_5$). The difference between the MCNP6 reference and AGENT calculation for P_1 with the *K-J* polar angular quadrature set (0.35 %) provides better agreement than P_5 with the LM (8.52 %) and TY (8.67 %) polar angular quadrature set. These results show the accuracy of the MOC neutron transport codes that reduce computation time by half.

Table 5. Material compositions of the unreflected cylinders of uranyl-fluoride solutions in heavy water [17]

Unit cell region	Element	Number density [cm^3]
Fuel solution (UO_2F_2-D_2O)	^{234}U	$3.0660\ 10^{18}$
	^{235}U	$2.8030\ 10^{20}$
	^{238}U	$1.5751\ 10^{22}$
	F	$5.9823\ 10^{20}$
	O	$3.2832\ 10^{22}$
	^{2}H	$6.3823\ 10^{22}$
	^{1}H	$6.4468\ 10^{20}$
Wall (type 321 stainless steel)	Fe	$5.9355\ 10^{22}$
	Cr	$1.6511\ 10^{22}$
	Ni	$7.7203\ 10^{19}$
	Mn	$1.7363\ 10^{19}$
	Si	$1.6982\ 10^{19}$
Dry air	N_2	$3.2269\ 10^{19}$
	O_2	$8.6569\ 10^{18}$

University of Utah TRIGA Research Reactor (UUTR) Benchmark

The University of Utah 100 kWth TRIGA MARK-I reactor (UUTR) is a pool-type research reactor, cooled by natural convection. The UUTR operates for research, training, and educational purposes including irradiation of materials, neutron activation analysis, and reactor operator training. The UUTR is selected to verify the *K-J* polar angular quadrature set for the regions predominantly occupied by ^{1}H (light water) and ^{2}H (heavy water) at the same time. In the prior research, the UUTR was also chosen as a final benchmark to verify the accuracy of the higher order neutron anisotropic scattering in the AGENT neutronics code system; this is because the UUTR is a very heterogeneous reactor of varied geometry and material composition [11]. Specifically, the UUTR has a hexagonal core that consists of 38 stainless steel and 23 aluminum clad uranium-zirco-

Table 6. The k_{eff} of the unreflected cylinders of uranyl-fluoride solutions in heavy water benchmark

Method		P_0	P_1	P_2	P_3	P_4	P_5
AGENT with LM	k_{eff}	1.05031	1.05030	1.05109	1.05109	1.05113	1.05108
	Difference [%]	8.59	8.59	8.52	8.52	8.52	8.52
	CPU time (hrs)	0.4	0.5	0.6	0.6	0.7	0.7
AGENT with TY	k_{eff}	1.04861	1.04860	1.04939	1.04939	1.04943	1.04939
	Difference [%]	8.74	8.74	8.67	8.67	8.67	8.67
	CPU time (hrs)	0.4	0.5	0.6	0.6	0.7	0.7
AGENT with *K-J* in solution region and LM in wall/air region	k_{eff}	1.14500	1.14499	1.14586	1.14586	1.14592	1.14587
	Difference [%]	0.35	0.35	0.28	0.28	0.27	0.28
	CPU time (hrs)	0.4	0.5	0.6	0.6	0.7	0.7
MCNP6	kinf (reference)	1.14903 0.00005					
	CPU time (hrs)	4.5					
AGENT resolution parameters: 48 azimuthal angles, 2 polar angles, 0.02 cm ray separation, 40 boundary edges per side AGENT converging criteria: flux 10^{-6}, eigenvalue 10^{-6} Boundary condition: reflective & vacuum boundary condition MCNP6: 1.000.000 particles, 600 histories, ENF/B-VII.0 Difference (%) = absolute (100 × (k_{inf} (MCNP6) – k_{inf} (AGENT)) / (k_{inf} (MCNP6))) Computer: Intel Xeon 5660 processor, 2.8 Ghz speed		AGENT sub-meshing of the unit cells: 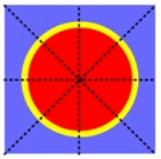					

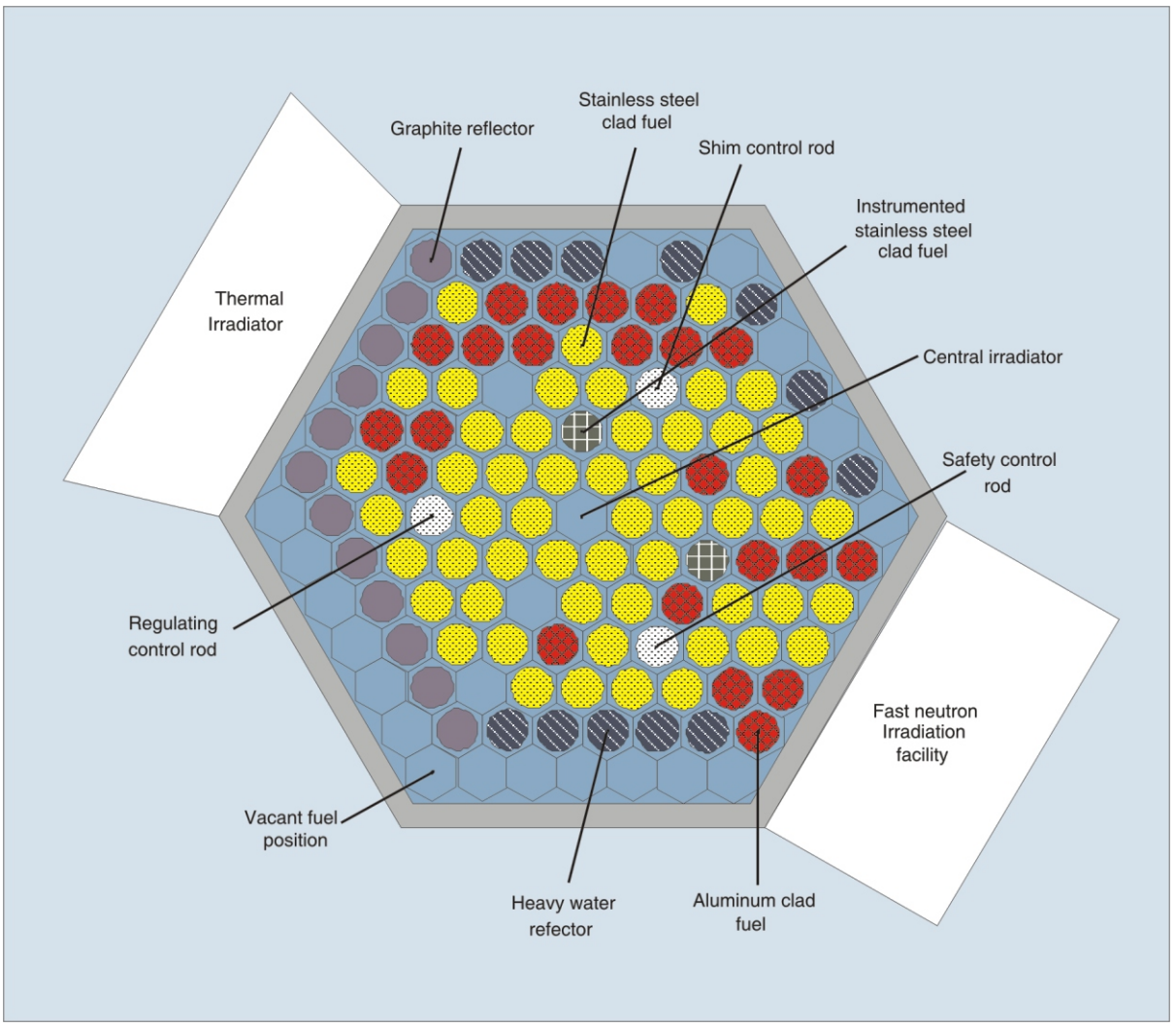

Figure 16. The 3-D UUTR core geometry [11]

nium-hydride fuel rods (8.5 wt. % uranium with <20 % enrichment), 12 graphite rods, 12 heavy water rods, and three control rods (safety, shim, and regulating control rods) made of powder boron carbide and housed in aluminum cladding [18]. The UUTR core has an in-core irradiation facility located in the central fuel position, the central irradiator (CI). The UUTR core also has two in-reflector irradiators that are external to the UUTR core: the thermal irradiator (TI) and the fast neutron irradiation facility (FNIF). The 3-D UUTR benchmark models the aforementioned features of the UUTR TRIGA MARK-I reactor with the control rods fully withdrawn. Figure 16 shows the UUTR core geometry.

The 3-D AGENT model of the UUTR includes the LM, TY, and *K-J* polar angular quadrature sets with two polar angles and seven energy group cross-sections calculated by SCALE 6.2.1. In the first and second cases of the UUTR benchmark, the LM and TY polar angular quadrature sets are applied to the whole UUTR region. The third case uses the *K-J* polar angular quadrature set with ^{1}H in the light water region, and LM in the other region. The fourth case uses the *K-J* polar angular quadrature set with ^{1}H in the light water regions, the *K-J* polar angle quadrature set with ^{2}H in the heavy water regions, and LM in the other regions.

Table 7 summarizes the AGENT k_{eff} for $P_0 \sim P_5$. Table 7 shows that the *K-J* polar angular quadrature set, with ^{1}H in the light water and ^{2}H in the heavy water region for lower P_n orders (P_0, P_1), is in better agreement with the reference MCNP6 calculations than for other quadrature sets (LM and TY) for all P_n orders ($P_0 \sim P_5$). Additionally, the *K-J* polar angular quadrature set, with ^{1}H in the light water and ^{2}H in the heavy water region with higher P_n order (P_5), provides the best agreement with the reference (0.001%). Computation times among the three polar angular quadrature sets (*K-J*, LM, and TY) are comparable, with no polar angular quadrature set demonstrating superior computational efficiency. All differences between the MCNP6 reference and AGENT calculations are less than 0.1 %, and differences between the MCNP6 and the *K-J* polar angular quadrature set with ^{1}H in the light water and ^{2}H in the heavy water region are 0.005 %. The difference between the MCNP6 reference and AGENT calculation for P_1 with the *K-J* polar angular

Table 7. The AGENT keff values for the 3-D UUTR benchmark

Method		P_0	P_1	P_2	P_3	P_4	P_5
AGENT with LM	k_{inf}	1.00883	1.00883	1.00883	1.00892	1.00892	1.00892
	Difference [%]	0.008	0.008	0.008	0.017	0.017	0.017
	CPU time [hrs]	9	12	14	16	18	20
AGENT with TY	k_{inf}	1.00970	1.00970	1.00970	1.00976	1.00976	1.00976
	Difference [%]	0.094	0.094	0.094	0.1	0.1	0.1
	CPU time [hrs]	9	12	14	16	18	20
AGENT with *K-J* in light water region and LM in other region	k_{inf}	1.00868	1.00868	1.00868	1.00874	1.00874	1.00874
	Difference [%]	0.007	0.007	0.007	0.001	0.001	0.001
	CPU time [hrs]	9	12	14	16	18	20
AGENT with *K-J* in light water region, *K-J* in heavy water region and LM in other region	k_{inf}	1.00870	1.00870	1.00870	1.00875	1.00875	1.00875
	Difference [%]	0.005	0.005	0.005	0.001	0.001	0.001
	CPU time [hrs]	9	12	14	16	18	20
MCNP6	k_{inf} (reference)	1.00875 0.00002					
	CPU time [s]	24.5					
AGENT resolution parameters: 24 azimuthal angles, 2 polar angles, 0.05 cm ray separation, 264 boundary edges per axial plane, 26 axial planes AGENT converging criteria: flux 10^{-6}, eigenvalue 10^{-6} Boundary condition: Vacuum boundary condition MCNP6: 1.000.000 particles, 600 histories, ENF/B-VII Difference (%) = absolute (100 × (k_{eff} (MCNP6) – k_{eff} (AGENT)) / (k_{eff} (MCNP6))) Computer: Intel Xeon x 5660 processor, 2.8 Ghz speed, OPENMP (multi-threading)		AGENT sub-meshing of the unit cell: 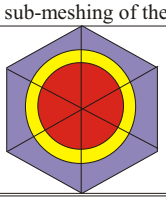					

quadrature set with ^{1}H in the light water and ^{2}H in the heavy water region (0.005 %) provides better agreement than P_5 with the LM (0.017 %) and TY (0.10 %) polar angular quadrature set. These results demonstrate that the accuracy of the MOC neutron transport codes can be improved with the *K-J* quadrature set.

However, the difference between the AGENT calculation for P_1 with the *K-J* polar angular quadrature set with ^{1}H in the light water only and with the *K-J* polar angular quadrature set with ^{1}H in the light water and ^{2}H in the heavy water region are just 0.002 %. This is because the difference in polar angular quadrature set weighting factors between the *K-J* polar angular quadrature set with ^{1}H and ^{2}H is small (see tab. 1). Additionally, the heavy water region (TI) applied by the *K-J* polar angular quadrature set with ^{2}H has a limited area compared with the whole core area to give have a high impact.

Figures 17 and 18 show the P_5 scalar neutron flux distributions of the *K-J* polar angular quadrature set for the 3-D UUTR for the thermal (10^{-5} eV~ 0.125 eV) and fast (1.356 10^6 eV~ 2 10^7 eV) energy groups, respectively. The P_5 scalar neutron flux distributions for the 3-D UUTR are split axially into four planes: (a), top plane with graphite and heavy water; (b), upper core plane with uranium-zirconium-hydride fuel rods; (c), lower core plane with uranium-zirconium-hydride fuel rods; and (d), bottom plane with graphite and heavy water. The thermal scalar neutron flux, fig. 17, is higher in the vacant fuel positions, central irradiator CI, the three fully withdrawn control rod locations, and the heavy water/graphite reflectors on the border of the core because the elastic scattering interactions with ^{1}H and ^{2}H thermalize the neutrons.

The CI shows the highest thermal scalar flux because the CI is fully surrounded by stainless steel clad fuel and is thus thermalizing more neutrons than anywhere else in the core. In the TI, the thermal scalar neutron flux is larger due to elastic scattering interactions with the row of graphite reflectors in front of the TI as well as the heavy water inside the TI thermalizing the neutrons. In contrast, the FNIF has a lower thermal scalar neutron flux because there are no reflectors separating the FINF from the core, and thus the neutrons from the core have less opportunity to undergo elastic scattering. The thermal scalar neutron flux is smallest in the fuel rods due to neutron absorption interactions, such as fission and radiative capture, by fuel materials.

The fast scalar neutron flux, fig. 18, is greatest within the fuel rods where fast neutrons are born from fission. Within the core, the magnitude of the fast scalar neutron flux is smaller in the empty water slot positions and the moderator-filled interstitial spacing between fuel rods due to elastic scattering interactions that thermalize the fast neutrons. The fast scalar neutron flux is also lower in the vacant fuel positions, CI, the three fully withdrawn control rod locations, and the heavy water/graphite reflectors on the border of the core because of both the elastic scattering interactions with ^{1}H and ^{2}H and the lack of fissile material to generate fast neutrons. The fast scalar neutron flux is larger in the FNIF because there are no graphite and heavy water reflectors in between the fuel rods and the FNIF, therefore the fast neutrons born from fission in the core travel directly to the FNIF with fewer chances to be elastically scattered. In contrast, there is a row of graphite reflectors in between the TI and the core, and thus fast neutrons will undergo elastic scattering be-

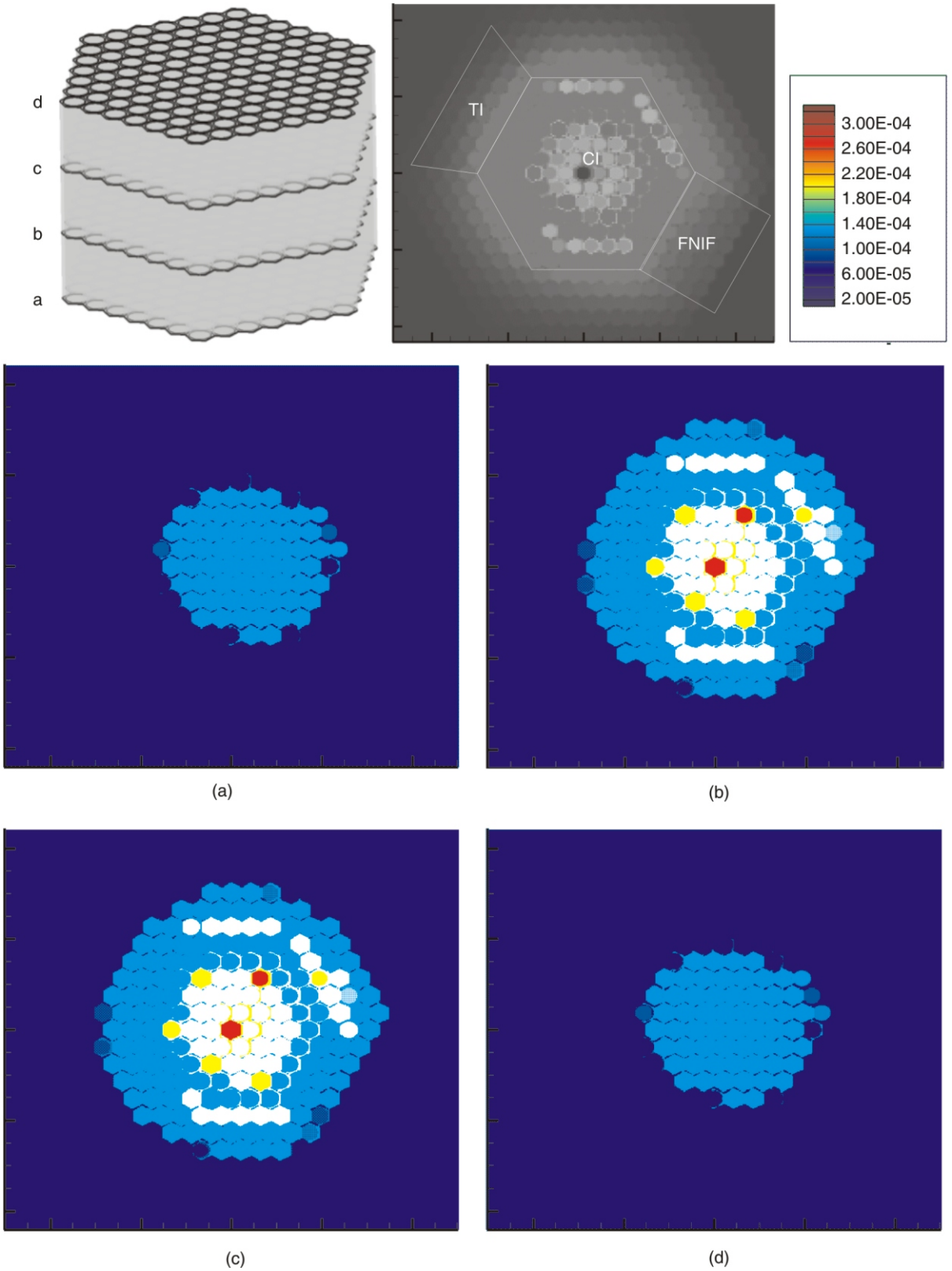

Figure 17. The AGENT 3-D UUTR P_5 scalar neutron flux distributions per axial plane with the *K-J* polar angular quadrature set with ^{1}H in the light water and ^{2}H in the heavy water region: Thermal energy group (10^{-5} eV~ 0.125 eV)

fore entering the TI. A steep gradient in the fast scalar neutron flux is observed at the boundary between the UUTR core and the moderator region external to the UUTR core, and the fast scalar neutron flux remains at a minimum because no neutrons are produced in the moderator.

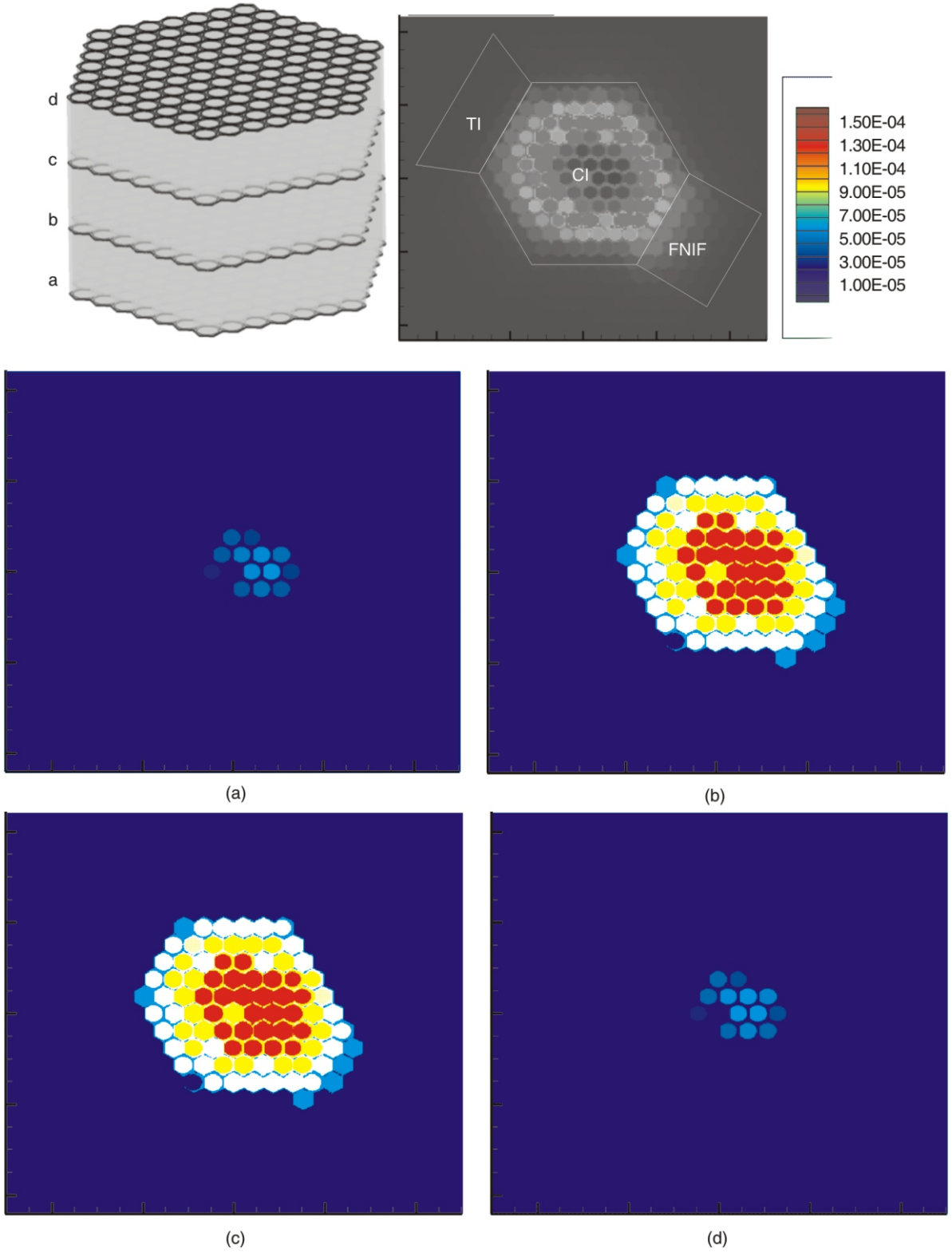

Figure 18. The AGENT 3-D UUTR P_5 scalar neutron flux distributions per axial plane with the *K-J* polar angular quadrature set with ^{1}H in the light water and ^{2}H in the heavy water region: Fast energy group (1.356 10^6 eV~ 2 10^7 eV)

Uncertainty analysis of the *K-J* polar angular quadrature set

The uncertainty analysis of the *K-J* polar angular quadrature remains for future work, and are is to be based on the uncertainties of the cross-sections for elastic neutron scattering derived from the ENDF-VIII.0 library that provides intrinsic certainty values, as illustrated with figs. 19 and 20. The suggested method for analyzing uncertainty of the *K-J* po-

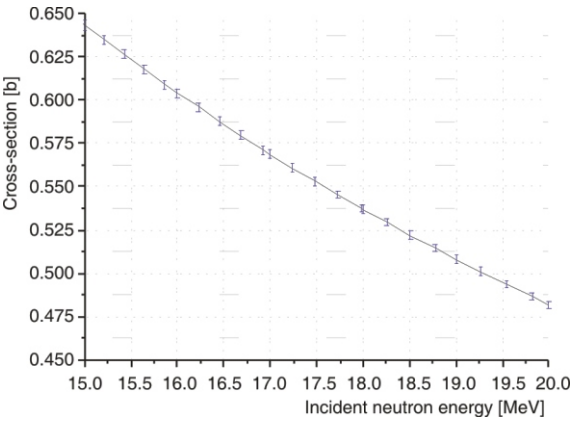

Figure 19. Elastic neutron scattering cross-sections with uncertainty for ^{1}H based on the ENDF-VII library: (15.0 MeV ~ 20.0 MeV)

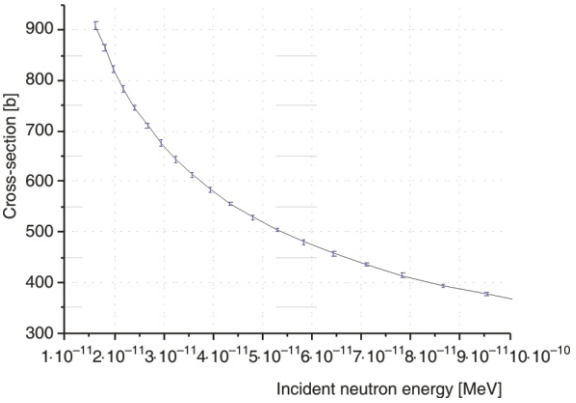

Figure 20. Elastic neutron scattering cross-sections with uncertainty for ^{1}H based on the ENDF-VIII library: (1.0 10^{-11} MeV~ 1 10^{-10} MeV)

lar angular quadrature set is the Monte Carlo sampling algorithm coupled with the AGENT system. The suggested algorithm is shown in fig. 21.

CONCLUSIONS

A novel polar angular quadrature set for the MOC- the Kim-Jevremovic polar angular quadrature set- is derived using the Evaluated Nuclear Data File (ENDF-VII) library [12], introduced into the state-of-the-art AGENT code, and then compared against the well-known Leonard and McDaniel and Tabuchi and Yamamoto polar angular quadrature sets for four different benchmark problems: square unit cell, the 2-D C5G7 benchmark, the unreflected cylinders of uranyl-fluoride solutions in heavy water, and the 3-D UUTR benchmark. Eigenvalues for the UO_2 unit cell, 2-D C5G7, the unreflected cylinders of uranyl-fluoride solutions in heavy water, and 3-D UUTR benchmarks show that the Kim-Jevremovic polar angular quadrature set provides the greatest agreement with the MCNP6 reference calculation for all P_n orders ($P_0 \sim P_5$). Kim-Jevremovic polar angular quadrature set with higher P_n order (P_5) shows best agreement with the reference for these benchmark problems. Finally, the Kim-Jevremovic polar angular quadrature set with P_1 order shows improved agreement with the MCNP6 reference calculations for all benchmark problems. These results demonstrate that, by using the Kim-Jevremovic polar angular quadrature set coupled with the MOC neutron transport codes, computation time can be greatly reduced.

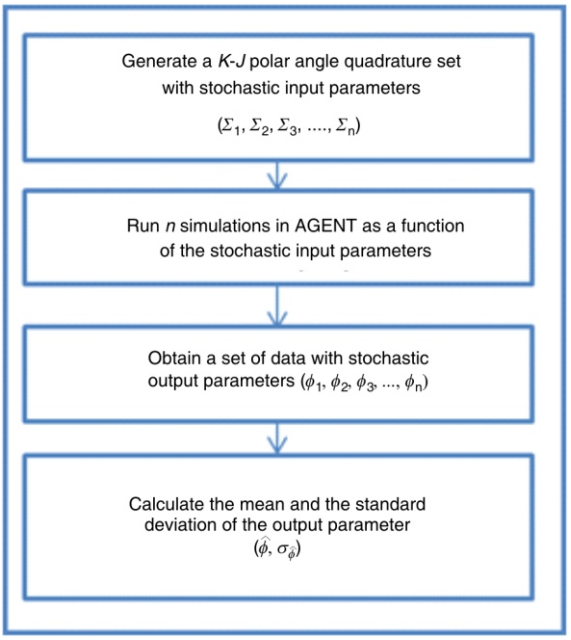

Figure 21. Monte Carlo sampling algorithm coupled with the AGENT code system

AUTHORS' CONTRIBUTIONS

D. Kim developed the K-J polar angle quadrature set and performed all benchmarks. L. I. Albright and B. L. Saenz made extensive contributions to the analysis of the results and preparation of the manuscript. Scientific supervision was done by T. Jevremovic.

REFERENCES

[1] Askew, J., A Characteristics Formulation of the Neutron Transport Equation in Complicated Geometries, 1972, United Kingdom Atomic Energy Authority
[2] Abramowitz, M., Stegun, I. A., Handbook of Mathematical Functions: with Formulas, Graphs, and Mathematical Tables, 55, 1964, Courier Corporation
[3] Halsall, M., CACTUS, A Characteristics Solution to the Neutron Transport Equations in Complicated Geometries, 1980, UKAEA Atomic Energy Establishment
[4] Leonard, A., McDaniel, C. T., Optimal Polar Angles and Weights for the Characteristics Method, Transactions of the American Nuclear Society, 1995, 73(CONF-951006)
[5] Yamamoto, A., *et al*., Derivation of Optimum Polar Angle Quadrature Set for the Method of Characteris-

tics Based on Approximation Error for the Bickley Function, *Journal of Nuclear Science and Technology, 44* (2007), 2, pp. 129-136
[6] Jevremovic, T., *et al*., ANEMONA-a Neutron Transport Code for General Geometry Reactor Assemblies Based on the Method of Characteristics and R-Function Solid Modeler, *Annals of Nuclear Energy, 28* (2001), 2, pp. 125-152
[7] Yamamoto, A., *et al*., Non-Equidistant Ray Tracing for the Method of Characteristics, 2005
[8] Marleau, G., *et al*., A User Guide for DRAGON Version 4. IGE-294, Ecole Polytechnique de Montreal, Institut de Genie Nucleaire Departement de Genie Mecanique (Aug. 26, 2016), 2011
[9] Ushio, T., *et al*., Neutron Anisotropic Scattering Effect in Heterogeneous Cell Calculations of Light Water Reactors, *Journal of Nuclear Science and Technology, 40* (2003), 7, pp. 464-480
[10] Jevremovic, T., *et al.*, Performance, Accuracy and Efficiency Evaluation of a Three-Dimensional Whole Core Neutron Transport Code AGENT. *Proceedings*, Int. Conf. ICONE14, Miami, Fla, USA, July. 2006.
[11] Kim, D., *et al*., Verification of the Accuracy of the Higher Order of Neutron Anisotropic Scattering in the AGENT Neutronics Code System, Annals of Nuclear Energy, 2017. 100: p. 73-90.
[12] Chadwick, M., *et al*., ENDF/B-VII. 0: Next Generation Evaluated Nuclear Data Library for Nuclear Science and Technology, *Nuclear Data Sheets, 107* (2006), 12, pp. 2931-3060
[13] Weisstein, E. W., Legendre Polynomial, 2002
[14] Herman, M., *et al*., Group, ENDF-6 Formats Manual Data Formats and Procedures for the Evaluated Nuclear Data File ENDF/B-VI and ENDF/B-VII. 2009, Brookhaven National Laboratory (BNL) National Nuclear Data Center
[15] Na, B. C., Benchmark on the VENUS-2 MOX Core Measurements, 2000
[16] Lewis, E., *et al*., Benchmark Specification for Deterministic 2-D/3-D MOX Fuel Assembly Transport Calculations Without Spatial Homogenization (C5G7 MOX), NEA/NSC, 2001
[17] Sapir, J. L., Unreflected Cylinders of Uranyl-Fluoride Solutions in Heavy Water, NEA/NSC/DOC(95)03, 1995. Volume II(HEU-SOL-THERM-020)
[18] ***, University of Utah Nuclear Engineering, License Renewal Application Updated Safety Analysis Report, June 2011

Received on October 21, 2018
Accepted on January 28, 2018

Донгхун КИМ, Лукас И. ОЛБРАЈТ, Бритни Л. САЕНЗ, Татјана ЈЕВРЕМОВИЋ

НОВА *K-J* ОПТИМИЗОВАНА РАСПОДЕЛА ПОЛАРНИХ УГЛОВА ЗА МЕТОДУ КАРАКТЕРИСТИКА ЗАСНОВАНА НА НЕУТРОНСКИМ ИНТЕРАКЦИЈАМА

Нова оптимизована расподела поларних углова названа *K-J* (Ким-Јевремовић) је специфично развијена за коришћење у неутронској методи карактеристика. Расподела је заснована на анизотропном расејању неутрона чије су вредности пресека евалуиране према ENDF-VII библиотеци неутронских пресека. Ова нова расподела поларних углова тестирана је коришћењем познатог нумеричког кода AGENT и у поређењу са MCNP6 на следећим геометријама: ћелија са горивом од UO_2, познати C5G7 бенчмарк, нерефлектовани цилиндар испуњен раствором уранил-флуорида у тешкој води, и реакторско језгро истраживачког реактора на Универзитету у Јути, 100 kW термичких TRIGA MARK-1. Ова поређења показују да нова расподела поларних углова даје боље слагање резултата са MCNP6 него друге до сада коришћене расподеле поларних углова за низак ред развоја анизотропног расејања у Болцмановој једначини неутронског транспорта. Овај рад укључује комплетно извођење *K-J* расподеле поларних углова и анализу поменутих бенчмарк тестова.

Кључне речи: AGENT нумерички програм, метода карактеристика, неутронско анизотропно расејање, расподела поларних углова, C5G7 бенчмарк, TRIGA